The Astrophysical Journal Supplement Series **175** (2008) 314-355 doi:10.1086/525025

The VSOP 5 GHz Active Galactic Nucleus Survey. V. Imaging Results for the Remaining 140 Sources

R. Dodson,[1,2] E. B. Fomalont,[3] K. Wiik,[1,4] S. Horiuchi,[5,6,7,8] H. Hirabayashi,[1,9] P. G. Edwards,[1,10] Y. Murata,[1,9] Y. Asaki,[1,9] G. A. Moellenbrock,[1,11] W. K. Scott,[12] A. R. Taylor,[12] L. I. Gurvits,[13] Z. Paragi,[13,14] S. Frey,[14,15] Z.-Q. Shen,[1,16] J. E. J. Lovell,[1,10,17] S. J. Tingay,[6,7,18] M. J. Rioja,[2] S. Fodor,[6,19] M. L. Lister,[20] L. Mosoni,[15,21] G. Coldwell,[22] B. G. Piner,[19] and J. Yang[13,16]

[1] Institute of Space and Astronautical Science, Japan Aerospace Exploration Agency, 3-1-1 Yoshinodai, Sagamihara, Kanagawa 229-8510, Japan.

[2] Observatorio Astronómico Nacional, Apartado 112, E-28803, Alcala de Henares, Spain.

[3] National Radio Astronomy Observatory, 520 Edgemont Road, Charlottesville, VA 22903.

[4] Tuorla Observatory, University of Turku, Väisäläntie 20, FIN-21500 Piikkiö, Finland.

[5] National Astronomical Observatory, 2-21-1 Osawa, Mitaka, Tokyo 181-8588, Japan.

[6] Jet Propulsion Laboratory, 4800 Oak Grove Drive, Pasadena, CA 91109.

[7] Centre for Astrophysics and Supercomputing, Swinburne University of Technology, P.O. Box 218, Hawthorn, Vic. 3122, Australia.

[8] Canberra Deep Space Communication Complex, P.O. Box 1035, Tuggeranong, ACT 2901, Australia.

[9] Department of Space and Astronautical Science, School of Physical Sciences, The Graduate University for Advanced Studies, 3-1-1 Yoshinodai, Sagamihara, Kanagawa 229-8510, Japan.

[10] Australia Telescope National Facility, Commonwealth Scientific and Industrial Research Organization, P. O. Box 76, Epping NSW 2122, Australia.

[11] National Radio Astronomy Observatory, P.O. Box 0, Socorro, NM 87801.

[12] Physics and Astronomy Department, University of Calgary, 2500 University Dr. NW, Calgary, AB T2N 1N4, Canada.

[13] Joint Institute for VLBI in Europe, P.O. Box 2, 7990 AA, Dwingeloo, Netherlands.

[14] MTA Research Group for Physical Geodesy and Geodynamics, P.O. Box 91, H-1521 Budapest, Hungary.

[15] FÖMI Satellite Geodetic Observatory, P.O. Box 585, H-1592, Budapest, Hungary.

[16] Shanghai Astronomical Observatory, Chinese Academy of Sciences, 80 Nandan Lu, Shanghai 200030, China.

[17] School of Mathematics and Physics, University of Tasmania, Private Bag 21, Hobart, Australia.

[18] Department of Imaging and Applied Physics, Curtin University of Technology, Perth, Australia.

[19] Physics Department, Whittier College, 13406 East Philadelphia, P.O. Box 634, Whittier, CA 90608-4413.

[20] Department of Physics, Purdue University, West Lafayette, IN 47907.

[21] MTA Konkoly Observatory, P.O. Box 67, H-1525, Budapest, Hungary.

[22] Observatorio Astronómico de la Universidad Nacional de Córdoba, Argentina.

Received 2007 August 22; accepted 2007 October 29; published 2008 April

ABSTRACT
In 1997 February, the Japanese radio astronomy satellite *HALCA* was launched to provide the space-bourne element for the VLBI Space Observatory Program (VSOP) mission. Approximately 25% of the mission time was dedicated to the VSOP survey of bright compact active galactic nuclei (AGNs) at 5 GHz. This paper, the fifth in the series, presents images and models for the remaining 140 sources not included in the third paper in the series, which contained 102 sources. For most sources, the plots of the (u, v)coverage, the visibility amplitude versus (u, v)distance, and the high-resolution image are presented. Model fit parameters to the major radio components are determined, and the brightness temperature of the core component for each source is calculated. The brightness temperature distributions for all of the sources in the VSOP AGN survey are discussed.

Subject headings: galaxies: active; radio continuum: galaxies; surveys

1. INTRODUCTION

The *Highly Advanced Laboratory for Communications and Astronomy* (*HALCA*) radio astronomy satellite was launched by the Institute of Space and Astronautical Science in 1997 February to participate in Very Long Baseline Interferometry (VLBI) observations with arrays of ground radio telescopes. *HALCA* provides the longest baselines of the VSOP, an international endeavor that has involved over 28 ground radio telescopes, five tracking stations, and three correlators (Hirabayashi et al. 1998, 2000a). *HALCA* was placed in an orbit with an apogee height above the Earth's surface of 21,400 km, a perigee height of 560 km, and an orbital period of 6.3 hr. During the 7 years of *HALCA*'s mission lifetime, about 75% of observing time was used for projects selected by international peer review from open proposals submitted by the astronomical community in response to announcements of opportunity. This part of the mission's scientific program constituted the general observing time (GOT). The remaining observing time was devoted to a mission-led survey of active galactic nuclei (AGNs) at 5 GHz: the VSOP Survey Program. The major goal of the Survey was to determine the statistical properties of the submilliarcsecond structure of a complete sample of AGNs (Hirabayashi et al. 2000b, hereafter Paper I; Fomalont et al. 2000a).

Following the end of the formal international mission period in 2002 February, the Japanese-dominated effort continued survey observations until 2003 October, when *HALCA* lost its attitude control capability. This occurred well after the end of the original planned mission lifetime.

This paper is the fifth in the series of VSOP Survey-related papers. Scott et al. (2004, hereafter Paper III) contains the results for 102 sources which were observed and reduced before 2001 October. Horiuchi et al. (2004, hereafter Paper IV) analyzed the cumulative visibilities of those sources to obtain the "typical source structure." This paper contains the additional 140 survey sources which were successfully observed by VSOP and completes the survey program observing results. The brightness temperature properties of the entire sample of sources are discussed.

2. THE OBSERVATIONS

The VSOP mission and the 5 GHz AGN Survey are fully discussed in Hirabayashi et al. (1998, 2000a), Paper I, and Fomalont et al. (2000b). Briefly, in order to be included in the VSOP Survey, a source was required to have

1. a total flux density at 5 GHz, $S_5 \geq 5.0$Jy,
2. a total flux density at 5 GHz, $S_5 \geq 0.95$Jy, a spectral index $\alpha \geq -0.45$($S \propto \nu^{\alpha}$), and a Galactic latitude $|b| \geq 10^{\circ}$.

The finding surveys from which sources were selected were primarily the Green Bank GB6 Catalog for the northern sky (Gregory et al. 1996), and the Parkes-MIT-NRAO (PMN) Survey (Lawrence et al. 1986; Griffith & Wright 1993) for the southern sky. The 402 sources satisfying these criteria compose the VSOP source list (Paper I). As this source list was compiled from single-dish catalogs, some of the selected sources would not be detectable by *HALCA* due to insufficient correlated flux density on baselines longer than about 1000 km. Therefore, sources with declination >–44° were observed in a VLBA prelaunch survey (VLBApls; Fomalont et al. 2000b) and a cutoff criterion, a minimum flux density of 0.32 Jy at 140 Mλ, was established for inclusion of a source in the VSOP Survey (Fomalont et al. 2000a). For sources south of –44°, this cutoff could not be determined, so all sources were included for *HALCA* observations. We find that 14 of these 24 southern sources observed have no detectable flux density on baselines to *HALCA*. Of the 402 sources in the complete sample, 294 were selected for VSOP observations, and this sample is designated as the VSOP Source Sample (VSS; Paper I; Edwards et al. 2002).
Observations of the VSS began in 1997 August, with the final observations being made in 2003 October when a second of the four *HALCA* momentum wheels became nonfunctional. Despite heroic attempts to heat up and free this reaction wheel throughout 2004, no further observations were possible. Of the VSS sample of 294 sources, all but 29 were observed. Details of the final status, the latest values of total density flux at 5 GHz, the redshift, relevant references, best-fit (or lower-limit) observer frame brightness temperatures of the core, detected area, and flux density on the longest baselines can be found in Table 1.

TABLE 1
VSOP AGN Survey Source List

A typical VSOP Survey observation used about three ground telescopes and *HALCA*, co-observing for up to ~6 hr. Ground radio telescopes that made the largest contributions to the Survey Program observations include the VLBA (US), Mopra (Australia), Hartebeesthoek (South Africa), Sheshan (China), Hobart (Australia), Kashima (Japan), Usuda (Japan), Ceduna (Australia), Kalyazin (Russia), and Noto (Italy). Other participants were the Green Bank 43 m (US), ATCA (Australia), Effelsberg (Germany), Arecibo (Puerto Rico), Torun (Poland), Onsala (Sweden),

VLA (US), Jodrell Bank MkII (UK), and Medicina (Italy). Further details are available in Dodson et al. (2006).
The VSOP survey observations were made at 5 GHz, with two left circularly polarized 16 MHz intermediate-frequency (IF) bandwidths, sampled with 2 bits (Hirabayashi et al. 2000a). GOT observations of survey sources which were made with a similar configuration were also included (see Paper III for discussion of this). Data were usually correlated at either the Dominion Radio Astrophysical Observatory (DRAO) Penticton correlator (Carlson et al. 1999) or the National Astronomical Observatory of Japan (NAOJ) Mitaka correlator (Shibata et al. 1998), with one non-GOT experiment processed at the Socorro correlator (Napier et al. 1994) along with two dozen GOT extractions (see Paper I; Scott et al. 2004 for details) and a test experiment in the data presented here. After correlation, the data were sent to the Institute of Space and Astronautical Science (ISAS) for distribution to the Survey Reduction Team members. The subset of those members who contributed the reductions that appear in this paper are represented in the author list.

3. DATA REDUCTION

Analysis of the data has been described elsewhere (Lovell et al. 2004) and hence is only briefly outlined here. The data were imported into AIPS (Greisen 1988), amplitude calibrated (with the measured or expected system temperature and, if needed, the autocorrelation normalized), then fringe fitted. A check of the amplitude calibration of the ground telescopes was made by observing a nearby calibrator source for about 5 minutes during the experiment. Because *HALCA* could not slew quickly between sources, its amplitude calibration could not be checked using a bright astronomical source. It was found, however, to be quite stable. Nevertheless, the amplitude calibration was entirely derived from the measured or expected gains for both *HALCA* and a number of ground antennas, which can be very uncertain. In Paper III great effort was spent in measuring an absolute correction for the flux scale of the Survey, in comparison with that of the VLBApls. In the data set presented here, we have fewer GOTs and a smaller overlap with the VLBApls, so such an approach was not possible. Therefore, we have assumed that the same correction (that the Survey experiments underestimate the flux densities by a factor of 0.83 ± 0.05compared to the VLBApls) can be made for these experiments. The amplitude scale errors were estimated as 20%, via the same comparison. After satisfactory delay and rate calibration, the data for all spectral channels were summed to a single channel per 16 MHz subband (i.e., two) and exported to DIFMAP (Shepherd 1997) for self-calibration and model fitting. Scripts were used as much as possible to ensure that the methods were standardized.
The results of, and supporting documentation for, the data reduction can be found on the project Web site.[23] The raw and calibrated data are available from ISAS on request.
Most VSS sources have been imaged with previous ground VLBI observations (including the VLBApls, which was specifically designed to add the lower resolution data to the VSOP Survey), and consistency of the VSOP image with these other images was used to constrain the cleaning and modeling. Where no supporting information was available, the models are relatively conservative.
For the entire VSOP Survey program, 265 of the 294 sources were observed. The observations that are reported in this paper are listed in Table 2, which includes source names, experiment code, ground radio telescopes, tracking stations and

correlator used, time over which fringes were detected, and the optical ID and redshift.

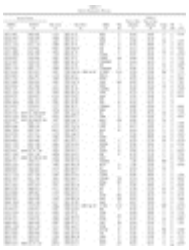

TABLE 2
Survey Experiment Details

For 50 of the observed sources, fringes to the spacecraft were not detected. Many of the sources were significantly resolved on shorter ground-only baselines, so the lack of space fringes (rms detection is typically 0.1 Jy) is consistent with the resolving structure seen on shorter baselines. However, for 23 of the observed sources where space fringes were not detected, ground observations suggested that the space baselines (typically greater than 150 Mλ) should have been detected. These observations are not included in the table of results, since the ground-only data provides no additional information about the source structure than is published elsewhere.

[23] Online at http://www.vsop.isas.jaxa.jp/survey.

4. THE RESULTS

4.1. The (u, v) Coverage, Visibility Amplitudes, and Images

The graphical results for most of the 140 additional Survey sources are given in Figure 1, which shows the (u, v) coverage, the visibility amplitude versus projected (u, v) distance, and the image displayed in contour form, with one row per source. The (u, v) distance is plotted in Mλ, the flux density in janskys, and the image in milliarcseconds (mas). The J2000.0 name of the source is listed at the top left of each row, followed by the experiment name and the observation date. The peak brightness (*P*) in janskys per beam appears above the image plot, followed by the noise level (σ), and the beam (*B*) major and minor axes and the major axis position angle. The image σ is estimated from a Gaussian fit to the pixel flux density distribution, but in a few cases it had to be manually increased due to high sidelobes in the image. The lowest contours are at –3 σ (*dashed lines*) and 3 σ (*solid lines*), doubling thereafter. The images presented are all made with uniform weighting, which highlights the highest resolution structure. The weighting scheme for each source was selected to give the clearest image. Further details are to be found on the VSOP Survey Web site. The (u, v) coverage among the sources varies considerably, and this had significant impact on the quality, resolution, and dynamic range of the images. For sources which were so heavily resolved that no space fringes are detected and with limited ground baseline coverage, no graphical results are shown, although the indication of overall angular size is still presented in Table 3. Sources for which no conclusions could be drawn (J1218–4600, J1424–4913, and J2358–1020) are not included.

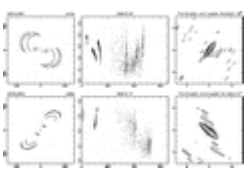

Figure 1.
Images of the Survey sources. For each source three separate panels are presented horizontally across the page. The first panel shows a plot of the (u, v) coverage, with *u* on the horizontal axis and v on the vertical axis. Both axes are

measured in units of Mλ, and the source and experiment name appears above. The second panel shows a plot of the amplitude of the visibilities (in janskys) vs. (u, v)radius, with the latter again measured in Mλ (time-averaged to 150 s). The date of observation appears above. For both of these plots only data that were actually used to make the final image are shown. In the third panel, a contour plot of the cleaned image is shown. The contour levels double with each level and start at 3 times the image rms, listed above the image, along with an additional negative contour, equal in magnitude to the minimum positive contour level. The peak flux, minimum contour level, and synthesized HPBW in milliarcseconds are shown on the top border.

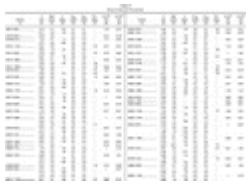

TABLE 3
Source Component Parameters

During deconvolution, we cross-checked our images with any other ground-based images of the source available, usually the VLBApls (Fomalont et al. 2000b). Although most AGNs are variable with time and frequency, these other images provided reasonable constraints to the VSOP source images, for example, the source extent and component locations. The space baselines have considerably higher noise compared to those on the ground because of the higher system temperature and smaller size of the *HALCA* antenna. Therefore, the space data were increased in weight to approximately the same significance as the ground data, in order to emphasize the highest resolution structure in the source. This was typically a factor of 10-20.
The VSOP data indicated the strength and approximate angular size of a core component, even if, in some cases, most of the most extended emission, shown with lower resolution images, was resolved out in the VSOP data. In general, the Survey data sets have a typical image fidelity of 20:1, and features less than 5% of the peak brightness should be treated with caution.

4.2. Model-Fitting and Brightness Temperature Determination

Once we obtained the best image for a source, consistent with the quality and quantity of the (u, v)coverage, we estimated the parameters for the major components of the source structure by Gaussian fitting: the integrated flux density, the centroid position, the major and minor axes, and orientation of the major axis. These parameters are listed in Table 3. In all cases, the radio core could be identified (it was usually the most compact component and often at one edge of the radio emission). Occasionally, high-resolution ground images at 15 and 23 GHz were also used to identify the location of the core. The radio core component is listed as the first component for sources which contain several components.
The brightness temperature of a component in the observer's frame is given by

$$T_b = \frac{S\lambda^2}{2k_B\Omega}, \qquad (1)$$

where S is the component flux density at wavelength λ, k_B is Boltzmann's constant, and $\Omega \approx 1.13(\theta_{maj})(\theta_{min})$ is the (Gaussian) weighted solid angle subtended by the component (which we have expressed in terms of the full width at half-maximum of the component major and minor axes). To convert to brightness temperature in the source frame, equation (1) is multiplied by $(1+z)$, where z is the source redshift.
For the radio core only, we carefully determined the best-fit angular size and its allowable range. To determine the range, we used the ad hoc method of varying critical parameters and estimating the range of angular size and flux density for each core component that is consistent with the data and its scatter (cf. Lovell et al. 2000). Two brightness temperatures are given for the radio cores in Table 3. First is the measured brightness temperature in the observer's frame, assuming that the core is a Gaussian-shaped component of the specified parameters. Sources for which only lower limits could be derived (i.e., unresolved sources) are marked with a greater than sign (>). The second brightness temperature is the lower limit of the brightness temperature (using the maximum angular size) converted to the *source frame*. If no redshift is available, zero redshift is assumed. These values are the lowest possible temperature compatible with the data. We list these as we feel that these are a more useful value than upper limits or best fits which depend critically on the interpretation of the very highest resolution data, which have the highest noise and the most sparse coverage.

4.3. Discussion of the Brightness Temperature Distributions

Histograms depicting the brightness temperature distribution in both the source and observer's frame for the sources presented here are shown in Figure 2. Here we have used the values for the best fits to the models (following the style of Paper III), rather than using the lower limits, in order to combine both data sets. (Sources with no measured redshift are not included in the plot of source-frame brightness temperatures.)

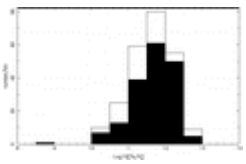

Figure 2.
Histogram of core brightness temperatures. *Left*: Core brightness temperature in the observer frame for the 239 survey sources with identified cores binned with $\log(T_b)$ on the abscissa, and the number per bin as the ordinate. We show the measured T_b where the source was resolvable with a filled bar, otherwise the lower limit to the T_b with an open bar. *Right*: T_b in the source frame for the subset of 222 sources which also have a measured redshift.

Most cores have $T_b > 10^{11}$ K, with approximately 56% of the sources having a measured brightness temperature in excess of 10^{12} K in the source frame, and approximately 30% of the sources having a measured brightness temperature greater than 10^{12} K in the observer's frame.
We find that overall, the mean brightness temperatures in our data are slightly lower than those in Paper III. This could be expected, given that our data include many more of the weaker sources (the median total flux density of sources in this paper is less

than one-half of the flux from those in Paper III) and a significant number with no space fringes, none of which were included in Paper III.
As we compare this result with other similar data sets (Tingay et al. 2001; Kovalev et al. 2005), we note that (as discussed in Paper III) the distribution in Tingay et al. (2001) matches that presented here once corrected by the factor $(1+z)^{1/2}/0.56$. This factor comes from the corrections for changing their results from an optically thick core model to a Gaussian and from comoving frame to the source frame. The distribution presented in Kovalev et al. (2005) is from VLBA observations at 15 GHz. They find also a median value of 10^{12} K, but the distribution toward 10^{13} and beyond is largely made up of lower limits, rather than actual measurements as we have here. We have compared the T_b for the source in common with Kovalev et al. (2005) by selecting the data with the closest observation dates. The T_b in the VSS tend to be higher, as expected, since the majority of the brightness temperatures in Kovalev et al. (2005) are lower limits, with a median ratio of 2.4. Detailed comparison of individual sources, in particular those with very different T_b, will be presented in a future paper (L. I. Gurvits et al., in preparation).
When looking at individual sources, we believe that the most useful number that can be provided is the lower limit to the brightness temperatures, which is that which *must* be generated by any proposed model or theory, rather than the brightest possible which *could* be required by any proposed model. The former will not produce the highest measured temperatures nor the most extended distribution. However, it will provide limits and distributions which must be achieved or exceeded. To probe the distribution of brightness temperatures, we prefer the approach taken in Paper IV, in which a cumulative visibility distribution was produced from all sources and a measurement of typical core sizes was fitted to these data. By this approach the very high errors at the extremes have reduced contributions.

4.4. Comments on Individual Sources

Survey sources that were not successfully scheduled are included in Table 1 with references (where they exist) to other VLBI observations marked with a dagger (†) on the experiment name.
The complete list of VSOP Survey observations is presented in Table 2. In addition, short notes on the sources are given. A general comparison is made with VLBI images from other observations, primarily the VLBApls (Fomalont et al. 2000b), US Naval Observatory Database (USNO; Fey et al. 1996; Fey & Charlot 1997, 2000), a space VLBI survey of Pearson-Readhead sources (VSOPPR; Lister et al. 2001), the VLBA 2 cm Survey (VLBA2cm1; Kellermann et al. 1998; Zensus et al. 2002; Kellermann et al. 2004; Kovalev et al. 2005), MOJAVE (Lister & Homan 2005), VLBA2cm2 (L. I. Gurvits et al., in preparation), results from VSOP observations of southern sources (VSOPsth; Tingay et al. 2002), and the VLBA Calibrator Survey (VCS; Beasley et al. 2002). Any significant differences are noted. The largest linear extent, or upper limit, is given.

1. *J0013+4051*.—The core is <0.2 mas in size, with extended emission to the northwest, as observed in other VLBA images.
2. *J0105+4819*.—The core is 0.2 mas in size. The more extended emission in other VLBA images that surrounds the core is undetected with the VSOP data.
3. *J0108+0135*.—The core is 0.2 mas in size and the location of the extended component is in agreement with other VLBA images.

4. *J0116–1136*.—Not detected on space baselines. The VSOP ground-only image and other VLBA images give a core size of ~0.5 mas in size.
5. *J0121+0422*.—The core is 0.4 mas in size. There is faint radio emission to the east, also seen with 15 GHz VLBA observations (Kellermann et al. 2004).
6. *J0125–0005*.—The core is 0.3 mas in size, and there is extended emission to the west.
7. *J0141–0928*.—Redshifts of both 0.733 and 0.44 have been reported (Stocke & Rector 1997). The core is 0.4 mas in size and nearly circular (Beasley et al. 2002).
8. *J0149+0555*.—The core is 0.4 mas in size, and the extended emission is similar to that seen with other VLBA images (Beasley et al. 2002).
9. *J0152+2207*.—The core is 0.4 mas in size and extended to the north. A faint extended component to the north, seen with other VLBA images, is present. (Fomalont et al. 2000b; Kellermann et al. 2004).
10. *J0204+1514*.—The core is <0.2 mas in size. The faint emission to the southeast is in the opposite direction of most of the jet emission, but the source structure evolution is complicated.
11. *J0204–1701*.—The core is 0.6 mas in size, and there is an extended component to the south.
12. *J0217+0144*.—The core is unresolved, <0.1 mas in size. The faint extended structure from lower resolution VLBA images is not detected.
13. *J0224+0659*.—The core is 0.3 mas in size. Emission to the west is also detected.
14. *J0231+1322*.—The core is ~0.4 mas in size. Faint emission to the northeast is also detected.
15. *J0237+2848*.—The core is <0.2 mas in size. Very extended emission to the north is detected.
16. *J0239+0416*.—The core is <0.2 mas in size. Extended emission to the northwest is detected.
17. *J0242+1101*.—The core is <0.2 mas in size. The emission to the southeast is clearly extended.
18. *J0253–5441*.—The core is 0.3 mas in size, in agreement with Ojha et al. (2005). The fainter component to the west is too weak to be detected by VSOP.
19. *J0259+0747*.—The core is 0.8 mas in size. The faint emission 3 mas to the south, seen in VLBA images, is not detected.
20. *J0303–6211*.—The core is 0.6 mas in size, extended east-west. There is a faint component 1.5 mas to the east.
21. *J0309–6058*.—Two small-diameter components, separated by 0.5 mas, are detected. The component to the northeast has the higher brightness temperature and is assumed to be the core.
22. *J0312+0133*.—The core is <0.2 mas in size. Faint emission to the east, seen with the VLBA, is just detected with VSOP.
23. *J0321+1221*.—The core is <0.15 mas in size. The extended component seen by VSOP is the inner part of a 20 mas jet seen by the VLBApls.
24. *J0336+3218*.—The core is 0.4 mas in size. Because of the lack of short spacings, none of the extended structure is detected by VSOP.
25. *J0339–0146*.—The core is 0.2 mas in size. The extended emission to the northeast is seen with other VLBA images.

26. *J0359+5057*.—The core is ~1.0 mas in size. The extended emission to the northeast, which extends 20 mas from the core in the VLBA images, is just detected by VSOP.
27. *J0402–3147*.—The core is 0.3 mas in size. The faint emission to the west is seen by the VLBApls.
28. *J0403+2600*.—The core is 0.35 mas in size. The extended emission to the west seen by the VLBApls is detected with VSOP. The model does not include the emission 15 mas to the north.
29. *J0406–3826*.—The core is <0.25 mas in size. The faint component to the west is found in the VLBApls, although the VCS image at 8 GHz has the fainter component to the east. This source is one of the most extreme of the intra-day variable sources (Kedziora-Chudczer et al. 1997).
30. *J0414+0534*.—A gravitationally lensed object with two major emission centers separated by 400 mas (Fomalont et al. 2000b). No image is shown, but the model fit of the Shanghai-to-Kashima baseline (20 Mλ) suggests a size of 1.6 mas for the more compact (probably southern) component.
31. *J0416–1851*.—The core is 0.5 mas in size. However, the flux density is about a factor 5-10 less than seen by other VLBI observations.
32. *J0424+0036*.—The core is 0.2 mas in size. The faint emission to the north is associated with more extensive emission seen in other VLBA images.
33. *J0424–3756*.—The core is 0.5 mas in size. The faint, extended component to the east is observed in other VLBA images.
34. *J0428–3756*.—The core is <0.5 mas in size. The faint, extended component to the east is observed in the VLBApls.
35. *J0433+0521*.—The VSOP observations suggest that the core is <0.3 mas in size. Only some of the extended structure to the west is imaged with VSOP.
36. *J0437–1844*.—The core is 0.7 mas in size, and the extended emission to the northwest is observed with other VLBA images. The space baselines are short, so the angular resolution is relatively low.
37. *J0442–0017*.—Not detected on space baselines, and no image is shown. The approximate size is 1.1 mas.
38. *J0449+1121*.—The VSOP data are consistent with a core <0.2 mas in size and extended emission to the east.
39. *J0450–8101*.—The core is <0.2 mas in size. There is extended emission on both sides of the core.
40. *J0508+8432*.—A redshift of 0.112 was initially reported for this object, but subsequently, an absorption system at 1.34 places a lower limit on the redshift (Stocke & Rector 1997). The core is 0.35 mas in size.
41. *J0509+0541*.—The core is <0.4 mas in size. The extended emission to the south and east is seen in the VLBApls.
42. *J0513–2159*.—The core is 1.1 mas in size with no detection on space baselines. No image is given.
43. *J0522–3627*.—The brightest component is identified as the core and is 0.4 mas in size. Most of the extended emission is to the northwest, with fainter emission to the southeast, which is identified as the core in Tingay & Edwards (2002). This component is <0.2 mas in size.
44. *J0530+1331*.—The space baselines suggest that the core component lies at the extreme southwest of the emission and contains about 0.22 Jy within a size <0.3 mas. Only a small part of the extended emission is contained in the other two model components.

45. *J0541–0541*.—The core is 1.2 mas in size, with no detection on space baselines. No image is given.
46. *J0607+6720*.—The emission is about 0.6 mas in size. It is best fit by two small components, each with a size <0.2 mas.
47. *J0614+6046*.—The core is 0.25 mas in size.
48. *J0626+8202*.—The core is 0.3 mas in size. The extended emission is complex and approximated by the additional two components. This source shows very interesting submilliarcsecond structure.
49. *J0646+4451*.—The core is identified with the fainter component to the west, based on the extended structure from VLBA images. The core is <0.2 mas in size.
50. *J0648–3044*.—The core is 0.4 mas in size. There is extended emission to the east, in agreement with other VLBA images.
51. *J0713+4349*.—The space baselines suggest a core component of 0.20 Jy with a size <0.2 mas. No image is given, since there is little ground baseline data.
52. *J0739+0137*.—The core is 0.2 mas in size. There is extended emission to the northwest.
53. *J0743–6726*.—The core is 0.7 mas in size. There is a slightly extended component 29 mas to the east. This structure agrees with Ojha et al. (2005).
54. *J0745+1011*.—The core is 0.4 mas in size. There is emission both north and south of the core. The VLBA images show that the source structure is variable and changes with frequency.
55. *J0750+1231*.—The core is 0.6 mas in size. There is extended emission to the east.
56. *J0808+4950*.—The core is 0.15 mas in size. Most of the extended emission is to the southeast, as seen in other VLBA images.
57. *J0820–1258*.—The core is <0.3 mas in size. There is extended emission to the east.
58. *J0825+0309*.—The core is <0.1 mas in size. There is limited data, so the faint extended emission to the north, seen in other VLBA images, is not present.
59. *J0831+0429*.—The core is 0.5 mas in size. There is extended emission to the east.
60. *J0842+1835*.—The southern, fainter component is the core with an angular size 0.3 mas. The northern component is only the inner part of the jet emission which extends over 10 mas from the core.
61. *J0854+5757*.—The core is 0.3 mas in size. Most of the extended emission is south of the core, with a hint of emission to the north.
62. *J0909+4253*.—The core is <0.15 mas in size. There is extended emission to the south.
63. *J0921–2618*.—Not detected on space baselines, and no image is given. The approximate angular size of the emission is 0.9 mas in position angle –17°, which agrees with the VLBApls results.
64. *J0948+4039*.—The core is 0.15 mas in size. There is extended emission to the southeast.
65. *J0956+2515*.—The core is <0.2 mas in size. The extended emission, some of which overlaps the core, lies to the west.
66. *J0958+4725*.—The core is 0.3 mas in size. There is no significant extended emission.
67. *J0958+6533*.—The core is <0.2 mas in size. There is extended emission to the northwest which agrees with Beasley et al. (2002).

68. *J1014+2301*.—No detection on space baselines. No image is shown, and the size of the emission is 0.8 mas.
69. *J1035–2011*.—The core is >0.15 mas in size. The faint extended emission is not detected in these observations.
70. *J1041+0610*.—The core is 0.5 mas in size. There is extended emission to the southeast.
71. *J1048–1909*.—The core is <0.1 mas in size. There is extended emission to the south.
72. *J1051+2119*.—The core is 0.2 mas in size. There is extended emission to the east.
73. *J1051–3138*.—The core is <0.2 mas in size. There is extended emission near and southwest of the core.
74. *J1058+1951*.—The source contains 0.07 Jy at 180 Mλ north-south, which is consistent with the VLBApls, with 0.4 Jy in a 0.9 mas north-south component.
75. *J1058–8003*.—The core is 0.4 mas in size. There is no indication of extended emission.
76. *J1118–4634*.—The core of 0.27 Jy is 0.7 mas in size. The total flux density is about 1.0 Jy (Tingay et al. 2003); hence, there may be additional extended emission.
77. *J1125+2610*.—The core is 0.8 mas in size, elongated in the direction of the more extended emission seen by the VLBApls.
78. *J1127–1857*.—The core is <0.2 mas in size. There is extended emission to the south.
79. *J1130–1449*.—The core is <0.2 mas in size. There is extended emission to the east. See Tingay et al. (2002).
80. *J1150–0023*.—No detection on space baselines, and no image is given. The core region contains about 0.13 Jy in a component <0.6 mas. See VLBApls for a model of the extended emission.
81. *J1153+4931*.—No detection on space baselines, and no image is given. The core emission is about 2.5 mas in the north-south direction
82. *J1153+8058*.—The core is 0.3 mas in size. There is faint emission south of the core.
83. *J1159+2914*.—The core is 0.3 mas in size. There is extended emission to the northeast.
84. *J1218–4600*.—No detectable flux density on ground baselines greater than ~100 Mλ. Hence, there is no image and model.
85. *J1224+0330*.—The core is <0.25 mas in size. There is extended emission to the west.
86. *J1224+2122*.—The core is <0.4 mas in size. There is extended emission to the north.
87. *J1257–3155*.—The core is <0.3 mas in size in the position angle of the extended emission seen by the VLBApls. There is a possible amplitude scaling error, so the core flux density may be a factor of 2 higher.
88. *J1305–1033*.—The core is <0.2 mas in size. No additional structure is seen with VSOP because of lack of short spacings.
89. *J1316–3338*.—The core is 0.3 mas in size. There is extended structure to the southwest and west.
90. *J1351–1449*.—Not detected on space baselines. No image is given. The core size is 1.0 mas.

91. *J1357+1919*.—We believe that the northernmost component is the core with a size of 0.7 mas. The component 2 mas southeast has a higher brightness temperature, but is probably a bright spot of the jet. More extended emission occurs further to the southeast.
92. *J1405+0415*.—The structure seen in the image with the full VSOP GOT 5 GHz data (Yang et al. 2006) is consistent with our result: the jet is extended ~15 mas to the west.
93. *J1415+1320*.—The core is 0.4 mas in size. There is extended emission at the same position as the core and also to the northwest.
94. *J1424–4913*.—No detectable flux density on global baselines greater than ~140 Mλ.
95. *J1427–4206*.—The core is 0.25 mas in size. There is extended emission to the north and east (Tingay et al. 2002).
96. *J1436+6336*.—The core is <0.25 mas in size. There is a stronger component north of the core and weaker emission to the south (VLBApls).
97. *J1504+1029*.—The core is <0.2 mas in size. There is extended emission to the east.
98. *J1516+0015*.—The core is <0.2 mas in size. Only space baselines are available; hence, none of the extended structure (to the northwest) is seen.
99. *J1522–2730*.—The core is 0.25 mas in size. There is extended structure to the west.
100. *J1550+0527*.—The core is <0.1 mas in size. There is extended structure to the north.
101. *J1557–0001*.—The core is 0.20 mas in size. No other significant extended structure is seen with VSOP.
102. *J1602+3326*.—The core is <0.2 mas in size. There is extended emission somewhat southeast of the core, but it is poorly defined because of the lack of short spacings.
103. *J1608+1029*.—The core is 0.5 mas in size. There is extended emission to the northwest.
104. *J1625–2527*.—The core is 0.5 mas in size. There is no significant extended structure.
105. *J1647–6437*.—The core is 0.9 mas in size. There is little (u, v) coverage, but no significant extended structure is seen.
106. *J1658+4737*.—Only space baselines. The core is 0.3 mas in size. The large-scale emission to the north is not seen.
107. *J1726–6427*.—There are no detections on space baselines, and no image is given. The Hartebeesthoek-Hobart baseline (145 Mλ) detects only 0.04 Jy.
108. *J1743–0350*.—The core is <0.15 mas in size and contains about 20% of the emission. The extended emission is somewhat south and east of the core.
109. *J1744–5144*.—There are no detections on space baselines, and no image is given. The Hartebeesthoek-Hobart baseline (145 Mλ) detects only 0.07 Jy.
110. *J1753+4409*.—There are only space baselines, and no image is given. The core is <0.15 mas in size.
111. *J1809–4552*.—The core is 0.5 mas in size and extended in PA –64°.
112. *J1824+1044*.—The core is 0.15 mas in size, and there is some extended structure to the north.

113. *J1837–7108*.—The core is 0.2 mas in size, and there is extended structure. We model this to the south; however, there is some ambiguity as to whether it is actually to the south or the north.
114. *J1842+7946*.—There are no detections on space baselines. The image and model show a core 0.3 mas in size and extended emission to the northwest up to 5 mas away.
115. *J1911–2006*.—The core is <0.2 mas in size. The flux density in the extended emission is higher and closer to the core than that in the VLBApls.
116. *J1912–8010*.—There are no detections on space baselines, and no image is given. The core is 0.6 mas in size, in general agreement with Ojha et al. (2005).
117. *J1925+2106*.—The core is 0.5 mas in size. There is extended emission to the west.
118. *J1927+7358*.—Lister et al. (2001) show the complete VSOP image. With more limited data, we assume that the core is the component at the northern edge of the source (component "D" in Lister et al.). Its flux density is 0.4 Jy with an angular size <0.4 mas. Only the two other components just south of the core are listed in our table. The extended emission to the south is not included.
119. *J1932–4546*.—There are no detections on space baselines, and no image is given. Hartebeesthoek-Hobart at 140 Mλ has 0.1 Jy correlated flux density. If one assumes a total flux density of 0.74 Jy (Tingay et al. 2003) in a circular Gaussian, the core size is 1.1 mas.
120. *J1937–3958*.—The core is 0.3 mas in size. There are no baselines less than 120 Mλ, so the extended structure seen with the VLBApls is not present.
121. *J1939–6342*.—Ojha et al. (2004) shows two components, separated by ~40 mas. The source is not detected on space baselines, and no image is given. Hartebeesthoek-Hobart at 140 Mλ has 0.1 Jy correlated flux density. If one assumes a total flux density of 1.0 Jy in the core component (the western of the 40 mas double), the core angular size is 1.1 mas.
122. *J1940–6907*.—There are no detections on space baselines. One component fit to the sparse ground data suggest a core size of 0.9 mas.
123. *J1955+5131*.—The core is 0.3 mas in size. There is extended emission toward the northwest.
124. *J2009–4849*.—There are no detections on space baselines. The core is 1.2 mas in size. The faint component to the west seen by Ojha et al. (2005) is below the VSOP detection level.
125. *J2011–1546*.—The core is <0.3 mas in size. There is a component just north of the core and a more extended component 2 mas north of the core.
126. *J2123+0535*.—The core is 0.3 mas in size. There is extended emission to the northeast.
127. *J2139+1423*.—The core is <0.3 mas in size. There is extended emission slightly to the east and to the south.
128. *J2148+0657*.—The core is 0.9 mas in size with no indication of more compact emission. There is faint extended emission to the southeast.
129. *J2151+0552*.—The core is <0.3 mas in size. There is extended emission over the core and to the west.
130. *J2152–7807*.—There are no detections on space baselines. The sparse data suggest a component of 0.9 mas in size, elongated in PA 33°.

131. *J2207–5346*.—The core component is 0.15 mas in size. There is extended emission toward the east.
132. *J2218–0335*.—The core component is 1.3 mas in size. Any compact core in this source is <0.1 Jy.
133. *J2232+1143*.—The core component is 0.4 mas in size. The complicated emission extends well to the south.
134. *J2236+2828*.—The core component is 0.5 mas in size. Any further compact component is <0.3 Jy.
135. *J2239–5701*.—There are no detections on space baselines, and no image is given. Hartebeesthoek-Hobart at 140 Mλ has 0.4 Jy correlated flux density. If one assumes a total flux density of 0.7 Jy (Tingay et al. 2003) in a circular Gaussian, the core size is 0.6 mas.
136. *J2246–1206*.—The core component is <0.2 mas in size. There is extended emission to the north.
137. *J2258–2758*.—The core component is 0.2 mas in size. There is extended emission to the south and east.
138. *J2336–5236*.—There are no detections on space baselines, and no image is given. Hartebeesthoek-Hobart at 140 Mλ has 0.15 Jy correlated flux density. If one assumes a total flux density of 1.63 Jy (Tingay et al. 2003) in a circular Gaussian, the core size is 1.2 mas.
139. *J2357–5311*.—The core component is 0.3 mas in size. There is extended emission to the southwest, in agreement with the lower resolution image of Shen et al. (1998).
140. *J2358–1020*.—There are space fringes implying a core component of 0.2 Jy within 0.2 mas. The ground data has amplitude scaling errors, so there is neither image nor model.

5. SUMMARY AND DISCUSSION

We have presented images, models and comments of the 140 sources which were observed as part of the VSOP Survey project that were not covered in Paper III. We have combined the brightness temperature measurements and limits found for the entire sample to produce the T_b distribution for the VSS.

We find that about one-half of the AGN sample of sources reported on in this paper have significant radio emission in the core component, with $T_b \geq 10^{12}$K in the source frame. Since the maximum brightness temperature one is able to determine using only ground-based arrays is of the order of 10^{12} K, our results confirm the necessity of using space VLBI to explore the extremely high brightness temperature regime. In addition, our Survey results clearly show that by using space VLBI with higher sensitivity, and somewhat higher resolution, the radio cores of many AGNs can be successfully imaged.

Because of the variability of many of the sources in the Survey sample, detailed spectral indices of the core components are difficult to determine. However, many of the sources were observed with the VLBA at 15 GHz as part of the VLBA2cm2 survey, and the spectral properties of the cores will be reported elsewhere (L. I. Gurvits et al., in preparation).

It was not possible to slew the *HALCA* satellite during the observing runs; therefore, *HALCA* was not able to participate in scans of fringe finders or flux calibrators. It is the absence of these which forces us to label a number of experiments with no space fringes as failures, when it could be the effects of the source structure. The design of

VSOP-2 will allow for fringe checks, and also phase-referencing experiments, to be performed (Hirabayashi 2000c).

The completion of this survey has been a Quixotic endeavor, and possibly "vino a dar en el más estraño pensamiento que jamás dio loco en el mundo; y fue que le pareció convenible y necesario, así para el aumento de su honra como para el servicio de su república, hacerse caballero andante" (Cervantes 1605).

We gratefully acknowledge the VSOP Project, which is led by the Institute of Space and Astronautical Science of the Japan Aerospace Exploration Agency, in cooperation with many organizations and radio telescopes around the world. R. D., K. J. W., G. A. M., and J. E. J. L. acknowledge support from the Japan Society for the Promotion of Science. R. D. acknowledges support as a Marie Curie fellow via EU FP6 grant MIF1-CT-2005-021873. Z. S. acknowledges support from NNSFC (10573029 and 10625314). W. K. S. wishes to acknowledge support from the Canadian Space Agency. S. H. acknowledges support through an NRC/NASA-JPL Research Associateship. S. F., Z. P., and L. M. acknowledge the OTKA T046097 grant received from the Hungarian Scientific Research Fund. S. F. and G. C. acknowledge the ASTRON and JIVE summer studentship programme. J. Y. acknowledges the CAS-UNAW cooperation programme in Radio Astronomy. This research has made use of data from the University of Michigan Radio Astronomy Observatory (UMRAO), which is supported by funds from the University of Michigan and the NSF, the United States Naval Observatory (USNO) Radio Reference Frame Image Database (RRFID), and the NASA/IPAC Extragalactic Database (NED), which is operated by the Jet Propulsion Laboratory, California Institute of Technology, under contract with the National Aeronautics and Space Administration. The NRAO is a facility of the National Science Foundation, operated under cooperative agreement by Associated Universities, Inc. The Australia Telescope Compact Array is part of the Australia Telescope, which is funded by the Commonwealth of Australia for operation as a National Facility managed by CSIRO. Meetings of the VSOP Survey Working Group were supported by EC FP6 Integrated Infrastructure Initiative, RadioNet (contract RII3-CT-2003-505818), JIVE, and the OAN.

REFERENCES

Beasley, A. J., Gordon, D., Peck, A. B., Petrov, L., MacMillan, D. S., Fomalont, E. B., & Ma, C. 2002, ApJS, 141, 13 First citation in article | CrossRef Link | NASA ADS | Order from Infotrieve

Carlson, B. R., Dewdney, P. E., Burgess, T. A., Casorso, R. V., Petrachenko, W. T., & Cannon, W. H. 1999, PASP, 111, 1025 First citation in article | CrossRef Link | NASA ADS | Order from Infotrieve

Cervantes, M., 1605, El ingenioso hidalgo don Quijote de la Mancha First citation in article

Dodson, R., et al. 2006, Proc. Science, 8, 070 First citation in article | Order from Infotrieve

Edwards, P. G., Hirabayashi, H., Fomalont, E. B., Gurvits, L. I., Horiuchi, S., Lovell, J. E. J., Moellenbrock, G. A., & Scott, W. K. 2002, 8th Asian-Pacific Regional Meeting, Vol. II, 375 First citation in article | NASA ADS

Fey, A. L., & Charlot, P. 1997, ApJS, 111, 95 First citation in article | CrossRef Link | NASA ADS | Order from Infotrieve

———. 2000, ApJS, 128, 17 First citation in article | CrossRef Link | NASA ADS | Order from Infotrieve

———. 1996, ApJS, 105, 299 First citation in article | CrossRef Link | NASA ADS | Order from Infotrieve

Fomalont, E. B., Frey, S., Paragi, Z., Gurvits, L. I., Scott, W. K., Taylor, A. R., Edwards, P. G., & Hirabayashi, H. 2000b, ApJS, 131, 95 First citation in article | CrossRef Link | NASA ADS | Order from Infotrieve

Fomalont, E., et al. 2000a, in Astrophysical Phenomena Revealed by Space VLBI, ed. H. Hirabayashi, P. G. Edwards, & D. W. Murphy (Sagamihara: ISAS), 167 First citation in article | NASA ADS

Gregory, P. C., Scott, W. K., Douglas, K., & Condon, J. J. 1996, ApJS, 103, 427 First citation in article | CrossRef Link | NASA ADS | Order from Infotrieve

Greisen, E. W. 1988, in Acquistion, Processing and Archiving of Astronomical Images, ed. G. Longo & G. Sedmak (Napoli: Osservatorio Astronomico di Capodimonte), 125 First citation in article | NASA ADS
Griffith, M. R., & Wright, A. E. 1993, AJ, 105, 1666 First citation in article | CrossRef Link | NASA ADS | Order from Infotrieve
Hirabayashi, H. 2000c, Adv. Space Res., 26, 751 First citation in article | CrossRef Link | NASA ADS | Order from Infotrieve
Hirabayashi, H., et al. 1998, Science, 281, 1825 First citation in article | CrossRef Link | NASA ADS | PubMed Abstract | Order from Infotrieve
Hirabayashi, H., et al. 1998, Science, 282, 1995 (erratum) First citation in article | CrossRef Link | NASA ADS | PubMed Abstract | Order from Infotrieve
———. 2000a, PASJ, 52, 955 First citation in article | NASA ADS | Inspec Abstract | Order from Infotrieve
———. 2000b, PASJ, 52, 997 (Paper I) First citation in article | NASA ADS | Inspec Abstract | Order from Infotrieve
Horiuchi et al. 2004, ApJ, 616, 110 (Paper IV) First citation in article | CrossRef Link | NASA ADS | Order from Infotrieve
Kedziora-Chudczer, L., Jauncey, D. L., Wieringa, M. H., Walker, M. A., Nicolson, G. D., Reynolds, J. E., & Tzioumis, A. K. 1997, ApJ, 490, L9 First citation in article | CrossRef Link | NASA ADS | Order from Infotrieve
Kellermann, K. I., Vermeulen, R. C., Zensus, J. A., & Cohen, M. H. 1998, AJ, 115, 1295 First citation in article | IOP Article
Kellermann, K. I., et al. 2004, ApJ, 609, 539 First citation in article | CrossRef Link | NASA ADS | Order from Infotrieve
Kovalev, Y. Y., et al. 2005, AJ, 130, 2473 First citation in article | IOP Article
Lawrence, C. R., Bennet, C. L., Hewitt, J. N., Langston, G. I., Klotz, S. E., Burke, B. F., & Turner, K. C. 1986, ApJS, 61, 105 First citation in article | CrossRef Link | NASA ADS | Order from Infotrieve
Lister, M. L., & Homan, D. C. 2005, AJ, 130, 1389 First citation in article | IOP Article
Lister, M. L., Tingay, S. J., Murphy, D. W., Piner, B. G., Jones, D. L., & Preston, R. A. 2001, ApJ, 554, 948 First citation in article | CrossRef Link | NASA ADS | Order from Infotrieve
Lovell, J., et al. 2000, in Astrophysical Phenomena Revealed by Space VLBI, ed. H. Hirabayashi, P. G. Edwards, & D. W. Murphy (Sagamihara: ISAS), 301 First citation in article | NASA ADS
———. 2004, ApJS, 155, 27 First citation in article | CrossRef Link | NASA ADS | Order from Infotrieve
Napier, P. J., Bagri, D. S., Clark, B. G., Rogers, A. E. E., Romney, J. D., Thompson, A. R., & Walker, R. C. 1994, Proc. IEEE, 82, 658 First citation in article | CrossRef Link | NASA ADS | Order from Infotrieve
Ojha, R., et al. 2004, AJ, 127, 3609 First citation in article | IOP Article
———. 2005, AJ, 130, 2529 First citation in article | IOP Article
Scott, W. K., et al. 2004, ApJS, 155, 33 (Paper III) First citation in article | CrossRef Link | NASA ADS | Order from Infotrieve
Shen, Z.-Q., et al. 1998, AJ, 115, 1357 First citation in article | IOP Article
Shepherd, M. C. 1997, in ASP Conf. Ser. 125, Astronomical Data Analysis Software and Systems VI, ed. J. A. Zensus, G. B. Taylor, & J. M. Wrobel (San Francisco: ASP), 77 First citation in article | NASA ADS
Shibata, K. M., Kameno, S., Inoue, M., & Kobayashi, M. 1998, in ASP Conf. Ser. 144, Radio Emission from Galactic and Extragalactic Compact Radio Sources, ed. J. A. Zensus, G. B. Taylor, & J. M. Wrobel (San Francisco: ASP), 397 First citation in article
Stocke, J. T., & Rector, T. A. 1997, ApJ, 489, L17 First citation in article | CrossRef Link | NASA ADS | Order from Infotrieve
Tingay, S. J., & Edwards, P. G. 2002, AJ, 124, 652 First citation in article | IOP Article
Tingay, S. J., et al. 2001, ApJ, 549, L55 First citation in article | CrossRef Link | NASA ADS | Order from Infotrieve
———. 2002, ApJS, 141, 311 First citation in article | CrossRef Link | NASA ADS | Order from Infotrieve
———. 2003, PASJ, 55, 351 First citation in article | NASA ADS | Inspec Abstract | ChemPort Abstract | Order from Infotrieve
Véron-Cetty, M.-P., & Véron, P. 2006, A&A, 455, 773 First citation in article | CrossRef Link | NASA ADS | Order from Infotrieve
Yang, J., Gurvits, L. I., Lobanov, A., Frey, S., & Hong, X. 2006, Proc. Science, 8, 086 First citation in article | Order from Infotrieve
Zensus, J. A., Ros, E., Kellermann, K. I., Cohen, M. H., Vermeulen, R. C., & Kadler, M. 2002, AJ, 124, 662 First citation in article | IOP Article